DOI: 10.13009/EUCASS2025-235
11TH EUROPEAN CONFERENCE FOR AERONAUTICS AND SPACE SCIENCES (EUCASS)

Transfers from Near Rectilinear Halo Orbits to Lunar Frozen Orbits

Guoliang Liang and Hongwei Yang*†*
** College of Astronautics, Nanjing University of Aeronautics and Astronautics,*
29 Jiangjun Road, Jiangning District, Nanjing, Jiangsu, The People's Republic of China,
lianggl@nuaa.edu.cn – hongwei.yang@nuaa.edu.cn
† Corresponding Author

Abstract
In this paper, a multi-maneuver strategy is proposed to transfer from a cislunar L2 near rectilinear halo orbit (NRHO) to a lunar frozen orbit (LFO). The maximum stretching direction is leveraged to determine the first maneuver, which makes the spacecraft leave NRHOs quickly. After a period of coast, the second maneuver is implemented to aim at the target orbit. Finally, the spacecraft is maneuvered to insert a LFO synchronized with the sun. The optimization results with different transfer windows in the high-fidelity model are given for the transfer from NRHOs to LFOs, which demonstrate the reliability of the proposed strategy.

1. Introduction

In recent years, there has been significant interest among researchers and engineers in lunar exploration. For example, the Artemis project planned by the National Aeronautics and Space Administration (NASA) is aimed at bringing people to moon again [1]. This makes the exploration of near lunar space a new focus. The periodic orbit of the near lunar space can not only facilitate the cislunar transfer or interplanetary exploration, but also act as a bridge to transfer to a circumlunar orbit [2][3]. The research on the transfer between near lunar space orbits could provide new mission orbits and enrich lunar exploration missions.
Near rectilinear halo orbit family is a subset of halo orbits [4], which is an important part of cislunar periodic orbits. In circular restricted three-body problem (CR3BP), NRHOs are regarded as the periodic orbit with nearly stable characteristic. Moreover, NRHOs have lower perilune altitude than other halo orbits. Due to the special location and characteristics of NRHOs in cislunar space, they play an important role in cislunar space. The Gateway space station on NRHO can be the launch platform for lunar landing missions and the Mars exploration missions can also benefit from NRHOs [5]. The large out-of-plane amplitudes relative to the lunar orbital plane provide an appropriate orbit for investigating the polar regions of the moon [6]. Moreover, NRHO can also serve as a mission orbit for relay communications satellites, which is important for lunar dorsal exploration [7]. Recently, there are many studies about the scientific issues related to NRHOs. Guzzetti et al. [8] analyzed the station keeping problem for spacecraft on NRHOs. Liu and Liu [9] proposed a notable method to compute multi-revolution NRHO under the ephemeris model. In addition, the orbital transfers are also commonly studied problems. Trofimov et al. [10] studied the transfers between NRHOs and low-perilune orbits even the moon's surface. Lu et al. [11] designed a direct transfer method from an NRHO to a low lunar orbit and analyzed the results from multiple aspects. Oshima [12] proposed to use the vertically stable manifolds of planar Lyapunov orbits to significantly reduce the velocity increment for the transfers from an NRHO to a distant retrograde orbit.
The lunar frozen orbits are the orbits with the constant mean eccentricity, mean orbital inclination, and mean argument of perilune [13]. Due to their stable dynamics characteristics and excellent geometric properties, the LFOs have broad applications in lunar exploration missions [14] [15]. The LFO is also an outstanding choice for relay satellite's mission orbit. Compared to NRHOs, LFO better meet the constraints and requirements imposed on orbit design by short duration lunar dorsal relay support missions [16]. A Sun-synchronous LFO, when designed by integrating multiple perturbations, can enable the orbital plane of the relay satellite to meet the operational requirements of short-duration lunar far-side missions (e.g., Chang'e-6) without necessitating additional adjustments.
However, the NRHO, an orbit of critical significance, and the LFO, a promising orbit around moon with high potential, have received little research focus regarding the design of transfer trajectories between them. The study on

DOI: 10.13009/EUCASS2025-235

the transfer of the two orbits can not only expand the accessible region of NRHO, but also provide novel transfer method for LFO.
Therefore, this paper is intended to investigate the design of transfer trajectory from NRHOs to sun- synchronized LFOs. The L_2 southern 9:2 NRHOs are selected as the research object in this paper. The contributions of this paper are as follows: Firstly, a novel multi-impulse transfer trajectory design method utilizing the stretching directions is proposed. The method transforms the trajectory design problem to a constrained nonlinear programming problem. A global optimization is applied to find the optimal solution, which is the transfer trajectory with the minimum velocity increment. Secondly, the proposed method is applied under both CR3BP model and the high-fidelity model to design the transfer trajectories. Several transfer trajectories with different initial epochs are obtained and analyzed, which proved the effectiveness of the method.
The paper is organized as follows: in Section 2, the background information including CR3BP, the calculation of NRHOs and LFOs are introduced. In Section 3, the transfer trajectory design method is introduced in detail. The results and relative discussion are in Section 4. Finally, the conclusions of the paper are discussed in Section 5.

2. Background

2.1 Circular restricted three-body problem

The CR3BP is a typical and reasonable approximation to describe the motion in the Earth-Moon system. The spacecraft is considered as a mass point with negligible mass. It moves under the joint gravity of the Earth and the Moon, which have much greater masses than the spacecraft. In this problem, the Earth and Moon are assumed to move in a circle around their center of mass. The motion is described in the synodic coordinate system shown in Figure 1. The origin is located at the barycenter of the Earth-Moon system, the x-axis pointing from Earth to Moon, the z-axis pointing to the normal of the orbital plane, the y-axis meeting the right-hand rule with the other two axes. In order to simplify the computation, the non-dimensional equation is used to calculate the state of the spacecraft. The masses of Earth and Moon are denoted as m_1 and m_2 respectively. The mass parameter is expressed as $\mu=m_2 / (m_1 + m_2)$. In this coordinate system, the Earth is at the fixed position $[-\mu, 0, 0]^{\mathrm{T}}$, and Moon is located at $[1-\mu, 0, 0]^{\mathrm{T}}$ along the x-axis. The dynamic equations are written as

$$\begin{cases} \ddot{x} - 2\dot{y} = \dfrac{\partial \Omega}{\partial x} \\ \ddot{y} + 2\dot{x} = \dfrac{\partial \Omega}{\partial y} \\ \ddot{z} = \dfrac{\partial \Omega}{\partial z} \end{cases} \tag{1}$$

where x, y, z is the position vector components in three axes. The effective potential is denoted by

$$\Omega = \frac{1}{2}\left(x^2 + y^2\right) + \frac{1-\mu}{r_1} + \frac{\mu}{r_2} \tag{2}$$

The distances r_1 and r_2 from the spacecraft to Earth and Moon can be written by the formulas

$$\begin{aligned} r_1 &= \sqrt{\left(x+\mu\right)^2 + y^2 + z^2} \\ r_2 &= \sqrt{\left(x-1+\mu\right)^2 + y^2 + z^2} \end{aligned} \tag{3}$$

DOI: 10.13009/EUCASS2025-235

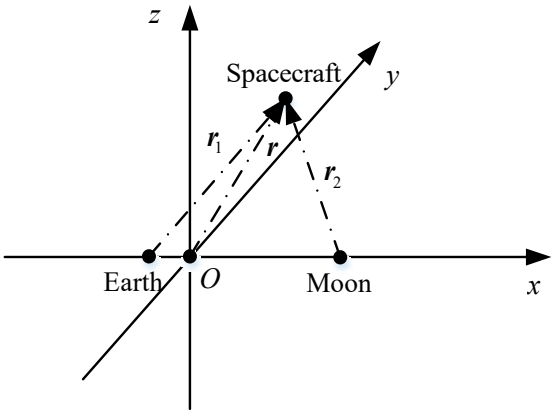

Figure 1: Synodic coordinate system in the Earth-Moon CR3BP

The physical parameters of the Earth–Moon system and the non-dimensional units are listed in Table 1.

Table 1: Physical parameter used in the dynamical model

Parameter	**Value**	**Meaning**
μ	1.21505856×10^{-2}	Mass ratio of the Earth–Moon system
LU (km)	3.61024835×10^{5}	Length unit
TU (s)	3.41493235×10^{5}	Time unit
VU (km/s)	1.05719468	Velocity unit

2.2 Near rectilinear halo orbits in CR3BP

In the CR3BP, halo orbits are one classical type of periodic orbits. They can be obtained by studying the bifurcation of Lyapunov orbits. They are three-dimensional orbits distributed near the small primary, L_1, and L_2 points. The approximate initial value of halo orbits can also be analytically determined; then, the differential correction method can be used to obtain the periodic orbit [17]. The whole halo orbit family can be obtained by the numerical continuation method with one converged solution. For halo orbits, the set of eigenvalues from the monodromy matrix is in the form: (1, 1, λ_1, $1/\lambda_1$, λ_2, $1/\lambda_2$). The stability indices can provide a measure of orbital stability. The stability indices are determined by the eigenvalues of the monodromy matrix:

$$\nu_i = \frac{1}{2}\left(\|\lambda_i\| + \frac{1}{\|\lambda_i\|}\right) \tag{4}$$

where λ_i is the eigenvalues of the monodromy matrix.

The near rectilinear halo orbits are a subset of halo orbits, whose projections in the x-z plane are approximately rectilinear. The NRHOs can be selected using the stability indices. They are stable or near stable. Southern L_2 NRHOs are shown in Figure 2.

DOI: 10.13009/EUCASS2025-235

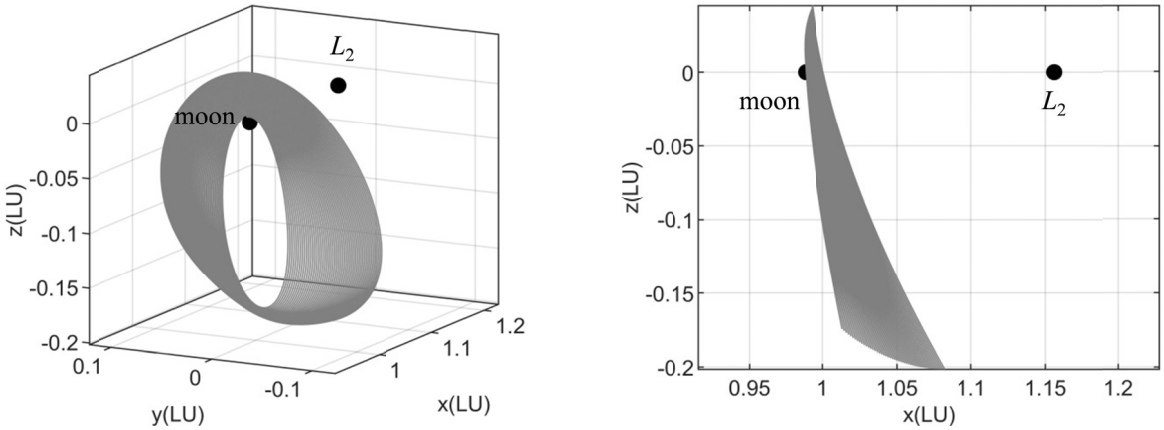

(a) 3D trajectories (b) *x*-*z* plane projections

Figure 2: Southern L2 NRHOs

When the orbital period of the spacecraft on a NRHO forms an integer ratio with the synodic period of the three-body system, this is defined as a synodic resonance. Specifically, a *p*: *q* resonant NRHO means the spacecraft completes *p* orbits in the NRHO while the Moon completes *q* orbits around Earth. In this study, the southern L_2 9:2 NRHO is selected to be the initial orbit of the transfer. The initial orbital characteristics of the selected NRHO are listed in Table 2.

Table 2: The initial orbital characteristics of 9:2 NRHO

***x* (LU)**	***z* (LU)**	**v_y (VU)**	***T* (TU)**
1.0218813	-0.18199999	-0.10295079	1.5092635

2.3 Lunar frozen orbit

In order to establish the dynamic equations of the system, it is necessary to define the Moon-Centered Inertial at Epoch (MCIE) coordinate system. The definition of the coordinate system is related to the epoch selected. Once the epoch is determined, the states of Earth and Moon are known. The origin of the coordinate system is located at the mass center of the Moon, with the *x*-axis pointing from the Earth to the Moon, the *z*-axis is aligned with the normal vector of the lunar orbit, the *y*-axis is determined using the right-hand rule. The coordinate system is shown in Figure 3.

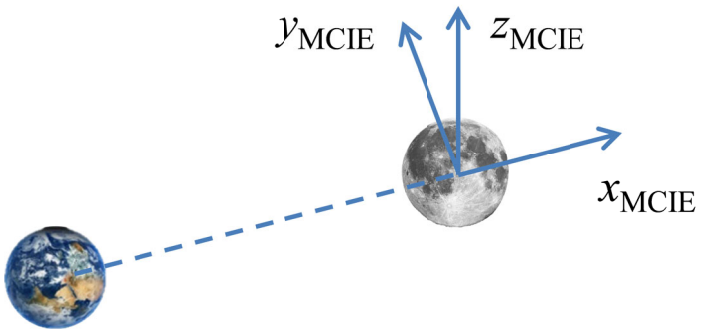

Figure 3: Moon-Centred Inertial at Epoch (MCIE) coordinate system

The dynamics equation is established including the perturbation of Earth's third body gravitation and J_2 of Moon in MCIE coordinate system. The von Zeipel method [13]is used to obtain the system mean dynamics equation after quadratic mean. The equation is denoted using the kepler orbital elements as follows

DOI: 10.13009/EUCASS2025-235

$$\begin{cases} \dot{a} = \dot{a}_1 + \dot{a}_2 + \dot{a}_{J_2} \\ \dot{e} = \dot{e}_1 + \dot{e}_2 + \dot{e}_{J_2} \\ \dot{I} = \dot{I}_1 + \dot{I}_2 + \dot{I}_{J_2} \\ \dot{\Omega} = \dot{\Omega}_1 + \dot{\Omega}_2 + \dot{\Omega}_{J_2} \\ \dot{\omega} = \dot{\omega}_1 + \dot{\omega}_2 + \dot{\omega}_{J_2} \\ \dot{M} = \dot{M}_1 + \dot{M}_2 + \dot{M}_{J_2} \end{cases} \tag{5}$$

where a is the semi-major axis; e is eccentricity; I is orbital inclination; Ω is right ascension of ascending node; ω is argument of perilune; M is mean anomaly. The subscript "1" denotes the first order term of the Earth's third body gravitation; the subscript "2" denotes the second order term of the Earth's third body gravitation; the subscript "J_2" denotes the 2nd-degree zonal harmonic representing the non-spherical gravity of the Moon. The expressions for the terms are:

$$\begin{cases} \dot{a}_1 = 0 \\ \dot{e}_1 = \dfrac{15n_m^2}{16n\mu} e\sqrt{1-e^2}\,\sin^2(I)\sin(2\omega) \\ \dot{I}_1 = \dfrac{15n_m^2}{16n\mu} \dfrac{e^2}{\sqrt{1-e^2}}\sin(2I)\sin(2\omega) \\ \dot{\Omega}_1 = \dfrac{3n_m^2}{8n\mu} \dfrac{\cos(I)}{\sqrt{1-e^2}}\left[-\left(2+3e^2\right)+5e^2\cos(2\omega)\right] \\ \dot{\omega}_1 = \dfrac{3n_m^2}{8n\mu} \dfrac{1}{\sqrt{1-e^2}}\left[\left(5\cos^2(I)+e^2-1\right)+5\left(\sin^2(I)-e^2\right)\cos(2\omega)\right] \\ \dot{M}_1 = \dfrac{3n_m^2}{8n\mu}\left[\left(3e^2+7\right)\left(3\cos^2(I)-1\right)+15\left(1+e^2\right)\sin^2(I)\cos(2\omega)\right] \end{cases} \tag{6}$$

$$\begin{cases} \dot{a}_2 = 0 \\ \dot{e}_2 = \dfrac{135n}{64\mu^2}\left(\dfrac{n_m}{n_m^*}\right)\left(\dfrac{n_m}{n}\right)^3 e\left(1-e^2\right)\sin^2(I)\cos(I)\sin(2\omega) \\ \dot{I}_2 = \dfrac{135n}{64\mu^2}\left(\dfrac{n_m}{n_m^*}\right)\left(\dfrac{n_m}{n}\right)^3 e^2\sin(I)\cos^2(I)\sin(2\omega) \\ \dot{\Omega}_2 = -\dfrac{9n}{128\mu^2}\left(\dfrac{n_m}{n_m^*}\right)\left(\dfrac{n_m}{n}\right)^3\left[2+33e^2-3\left(2-17e^2\right)\cos^2(I)+15e^2\left(1-3\cos^2(I)\cos(2\omega)\right)\right] \\ \dot{\omega}_2 = \dfrac{27n}{64\mu^2}\left(\dfrac{n_m}{n_m^*}\right)\left(\dfrac{n_m}{n}\right)^3\cos(I)\left[11\left(1-e^2\right)+5\cos^2(I)+5\left(\sin^2(I)-e^2\right)\cos(2\omega)\right] \\ \dot{M}_2 = -\dfrac{9n}{64\mu^2}\left(\dfrac{n_m}{n_m^*}\right)\left(\dfrac{n_m}{n}\right)^3\sqrt{1-e^2}\cos(I) \\ \left[3\left(13+22e^2\right)+\left(11+34e^2\right)\cos^2(I)+15\left(1+2e^2\right)\sin^2(I)\cos(2\omega)\right] \end{cases} \tag{7}$$

DOI: 10.13009/EUCASS2025-235

$$\begin{cases} \dot{a}_{J_2} = 0 \\ \dot{e}_{J_2} = 0 \\ \dot{I}_{J_2} = 0 \\ \dot{\Omega}_{J_2} = -\dfrac{3}{2}\dfrac{nr_m^2 J_2}{a^2\left(1-e^2\right)^2}\cos\left(I\right) \\ \dot{\omega}_{J_2} = -\dfrac{3}{4}\dfrac{nr_m^2 J_2}{a^2\left(1-e^2\right)^2}\left(1-5\cos^2\left(I\right)\right) \\ \dot{M}_{J_2} = -\dfrac{3}{4}\dfrac{nr_m^2 J_2}{a^2\left(1-e^2\right)^{3/2}}\left(1-3\cos^2\left(I\right)\right) \end{cases} \tag{8}$$

where n_m is the average orbital angular velocity of the Moon; n is the average orbital angular velocity of the spacecraft around the Moon; μ is the mass ratio coefficient of the Earth-Moon system, which is equal to that in CR3BP numerically; n_m^* is the average autorotation velocity of the Moon; r_m is the physical radius of the Moon; J_2=2.03×10^{-4}.

The lunar frozen orbit is defined as the orbit around the Moon with the constant mean eccentricity, mean orbital inclination and mean argument of perilune. That means it must satisfy the frozen condition

$$\begin{cases} \dot{e} = 0 \\ \dot{I} = 0 \\ \dot{\omega} = 0 \end{cases} \tag{9}$$

In order to satisfy the condition of eccentricity and inclination, the possible solutions can be calculated from eq. (5)-eq. (8), which is e=0, I=0 or sin2ω=0. The constraints on the spacecraft orbit in the first two cases are too strong. Therefore, the solution of sin2ω=0 is generally taken in engineering practice. That means the value of the argument of perilune can be determined

$$\omega = \pm\frac{\pi}{2} \tag{10}$$

If the dynamic model is simplified, which means only the first order term of Earth's third body gravity is considered, the frozen condition can be written as

$$\cos^2 I = \frac{3}{5}\left(1-e^2\right) \tag{11}$$

Another requirement is that the spacecraft must be synchronous with the Sun. In other words, the precession angular velocity of the right ascension of the ascending node (RAAN) of the orbital plane should equal the average angular velocity of the Sun's motion relative to the Moon. The precession of the orbital plane is primarily influenced by the combined effects of J2 term perturbation from the lunar non-spherical gravitational force and third-body gravitational perturbation from the Earth. This precession is reflected in the rate of change of the RAAN. Therefore, the Sun synchronous condition is that the RAAN precession rate matches the Sun's relative angular velocity:

$$\dot{\Omega} = \dot{\Omega}_1 + \dot{\Omega}_2 + \dot{\Omega}_{J_2} = n_{\text{sun}} \tag{12}$$

where n_{sun} = 1.99102 rad/s is the average angular velocity of the Sun.

When only the 1st order term of the Earth's third body gravitation is considered, the Sun synchronous condition can be simplified as

$$\dot{\Omega} = \frac{3}{4}\sqrt{\frac{3}{5}}\frac{n_m^2}{n\mu}\left(1+4e^2\right) = n_{\text{sun}} \tag{13}$$

Therefore, the eccentricity can be determined as

DOI: 10.13009/EUCASS2025-235

$$e^2 = \frac{1}{3}\sqrt{\frac{5}{3}}\frac{n\mu}{n_m^2}n_{\text{sun}} - \frac{1}{4} \tag{14}$$

Eq (11) and (14) can be used to determine the initial value of the lunar frozen orbit. If the parameter of orbital semi-major axis is determined, the shape of the orbit is determined. In order to facilitate measurement and control on the ground, the phase of the spacecraft should remain as stable as possible. The nodal period is defined as

$$T_p = \frac{2\pi}{\dot{\omega} + \dot{M}} \tag{15}$$

The nodal period is the time it takes for a spacecraft on a perturbed elliptical orbit to complete one revolution around a central celestial body. Therefore, if the nodal period of the spacecraft is accurately controlled to be equal to the measurement period, the spacecraft will be in the same phase for each measurement operated by ground station. Because the frozen condition constrains the derivative of the argument of perilune to be zero, the constraint can be written as

$$\dot{M} = \dot{M}_1 + \dot{M}_2 + \dot{M}_{J_2} = \frac{2\pi}{T_R} \tag{16}$$

where T_R is the period of measurement from ground station. For the computation of the initial value, the latter two terms could be ignored. The initial value of n can be obtained by substituting the eq. (6) into eq. (16).
However, the initial value is calculated in the dynamics only with 1st order term of the Earth's third body gravitation. In order to better satisfy the requirement of freezing and synchronization in the high-fidelity model, the J_2 term of the Moon and the second-order term of the third-body gravity also need to be taken into account. In the high-fidelity model, the orbital design problem is to solve the non-linear equations

$$\begin{cases} \dot{\Omega} = n_{sun} \\ \dot{\omega} = 0 \\ \dot{M} = 2\pi / T_R \end{cases} \tag{17}$$

In order to solve the equations, the differential correction method could be applied. First, the initial value should be determined. Then the simplified analytical partial derivative matrix is computed using dynamic equations where the 1st order term of the Earth's third-body perturbation is included. Finally, in the full perturbation model considering the non-spherical gravitational perturbation J2 term of the Moon, the first-order and second-order terms of the Earth's third-body gravitational perturbation, the method of differential correction is adopted to obtain high-precision numerical solutions. The variables to be solved is $\boldsymbol{x} = [n, e, \cos I]^{\mathrm{T}}$, and the target variables and their values are listed in eq. (17).
The initial values and the converged results in MCIE coordinate system are listed in Table 3

Table 3: The initial values and the converged results

Orbital element	initial value	converged results
semimajor axis, km	10003.061	9931.320
eccentricity	0. 778987	0.754818
inclination, deg	119.058	120.951

3. Multi-impulse transfer trajectory from an NRHO to a frozen orbit

The transfer trajectory design departing from an NRHO (Near Rectilinear Halo Orbit) to a frozen orbit involves three impulses. Initially, the first impulse is designed to initiate the spacecraft's departure from the NRHO. Then the spacecraft is free to coast for a period of time. Subsequently, the second impulsive maneuver is applied to aim for a target position on the frozen orbit. Finally, the last impulsive maneuver is performed to insert the spacecraft into the

DOI: 10.13009/EUCASS2025-235

frozen orbit. The entire trajectory design is formulated as a nonlinear programming problem. The transfer is optimized to find the minimum fuel consumption to complete the three maneuvers.

3.1 Fast away from the NRHO using stretching directions

Since NRHOs are near stable periodic orbits, using the invariant manifolds to depart from NRHO is difficult. On the one hand, the time cost of flight is substantial. On the other hand, it is difficult to substantially change the state of the spacecraft using only invariant manifolds. If the departing impulse is treated as a three-dimensional optimization variable, the nonlinearity of the problem will be intensified, making the problem more difficult to solve.
The concept of stretching directions is proposed to assess the impact of a maneuver [6]. Any velocity change along the maximum stretching direction can drive the spacecraft to deviate from the periodic orbit rapidly. The linear state transition matrix (STM) is used to assess the effect of initial deviations on the terminal states.

$$\Phi\left(t_f, t_0\right) = \frac{\partial x(t)}{\partial x_0} = \begin{bmatrix} \Phi_{r,r} & \Phi_{r,v} \\ \Phi_{v,r} & \Phi_{v,v} \end{bmatrix} \tag{18}$$

where t_0 and t_f are respectively the initial time and final time; x_0 is the initial state; $x(t)$ is the states at t_f. The impact of initial perturbation states on the perturbation of terminal states can be mapped by the STM. Therefore, the changes of the terminal states with given initial velocity perturbations can be obtained.

$$\Phi_{rv,v} = \begin{bmatrix} \Phi_{r,v} \\ \Phi_{v,v} \end{bmatrix} \tag{19}$$

where $\Phi_{rv,v}$ is one 6×3 dimensional sub-matrix of $\Phi(t_0, t_f)$. The changes of the terminal states can be regarded as the departure from the reference orbit. The sensitivity of the orbital state's changes at the final moment to initial velocity changes determines the efficiency of the maneuver moving away from the initial orbit. The sensitivity can be mapped by the magnitude of maximum stretching σ corresponding to the $\Phi_{rv,v}$. The maximum stretching σ is obtained from eigenvalue of the $\Phi_{rv,v}$.

$$\sigma_i = \sqrt{\lambda_i} \tag{20}$$

where λ_i is the eigenvalue of the $\Phi_{rv,v}$.
Carry out singular value decomposition to eq. (19)

$$U\Sigma V^{\mathrm{H}} = \Phi_{rv,v} \tag{21}$$

where Σ is a diagonal matrix combined with σ_i. V provides the direction information. Applying a velocity change along the component of V corresponding to the maximum σ_i, the states at the terminal moment takes the maximum change.

3.2 Design of the multi-impulse transfer trajectory

In this section, the multi-impulse transfer trajectory design problem is transformed to a constrained nonlinear programming problem. The first design variable is the phase of the initial state on the NRHO. In order to make the state easy to calculate, the variable is selected to be the flight time tof_0 from the initial point. The apolune is chosen to be the initial point. According to Section 3.1, the direction of the first impulse for spacecraft to departing the NRHO can be determined. Therefore, the design variable descends from three-dimensions to one dimension. The second variable is naturally the magnitude of the impulse maneuver dv_1. After a period time of flight tof_1, which is the third design variable, the spacecraft arrives at a new state. The second impulse maneuver $\boldsymbol{dv}_2$=[dv_{2x}, dv_{2y}, dv_{2z}]$^{\mathrm{T}}$ is operated to aim at the frozen orbit. Here, a necessary constrained local optimization is introduced. The design variable is the three- dimensional velocity increment. The spacecraft will reach the position of some point on frozen orbit after a period time of flight tof_2. Finally, the required three-dimensional velocity for insertion into the frozen orbit can be calculated with the arriving velocity and the targeting velocity on frozen orbit. According to Section 2.3, there are three orbital elements can be determined, while the other three orbital elements Ω, ω, and M are unknown. For some special missions, the three elements can be designed. For example, if the spacecraft orbital plane normal is

DOI: 10.13009/EUCASS2025-235

required to be designed at some angle to the Sun, the Ω can be designed. But in this study, there is no constraint on them. The specific location of the insertion point on the frozen orbit is also required to be optimize, which is corresponding to the three designed orbital elements. Therefore, the global design variables are

$$\boldsymbol{x}_G = \begin{bmatrix} tof_0 & tof_1 & tof_2 & \Omega & \omega & M & dv_1 \end{bmatrix} \tag{22}$$

In addition, constrained local optimization problems nested in global optimization are as follows

$$\boldsymbol{x}_L = \begin{bmatrix} dv_{2x} & dv_{2y} & dv_{2z} \end{bmatrix} \tag{23}$$

The local optimization objective is expressed as the magnitude of velocity increments, and the constraint is the magnitude of the difference of position as

$$\begin{aligned} &\text{Minimize}: y_L = f\left(\boldsymbol{x}_L\right) = \left\|\boldsymbol{dv}_2\right\| \\ &s.t. \quad \left\|\boldsymbol{r}_f - \boldsymbol{r}_{FO}\right\| = 0 \end{aligned} \tag{24}$$

where $\boldsymbol{r}_f$ is the state after spacecraft applied maneuver $\boldsymbol{dv}_2$ and time of flight; $\boldsymbol{r}_{FO}$ is the position on the frozen orbit, calculated by the orbital elements.
The global optimization objective is expressed as the sum of the magnitude of the velocity increments. The form is

$$\text{Minimize}: y_G = \left|dv_1\right| + y_L + \left\|\boldsymbol{v}_f - \boldsymbol{v}_{FO}\right\| \tag{25}$$

where $\boldsymbol{v}_f$ is the velocity of the corresponding state of $\boldsymbol{r}_f$; $\boldsymbol{v}_{FO}$ is the velocity of the corresponding state of the $\boldsymbol{r}_{FO}$. The global optimization problem can be solved by genetic algorithm.

4. Result and Discussion

Several solutions of transfer trajectories are calculated by selecting several initial epochs through the algorithm in section 3. The trajectories in Moon-centered J2000 frame (MCI) are calculated under the dynamics considering the gravity of Earth, Moon, the Sun, and Jupiter, which are as shown in the left part of Figure 4-Figure 6. The right part of Figure 4-Figure 6 are the trajectories calculated under the CR3BP.

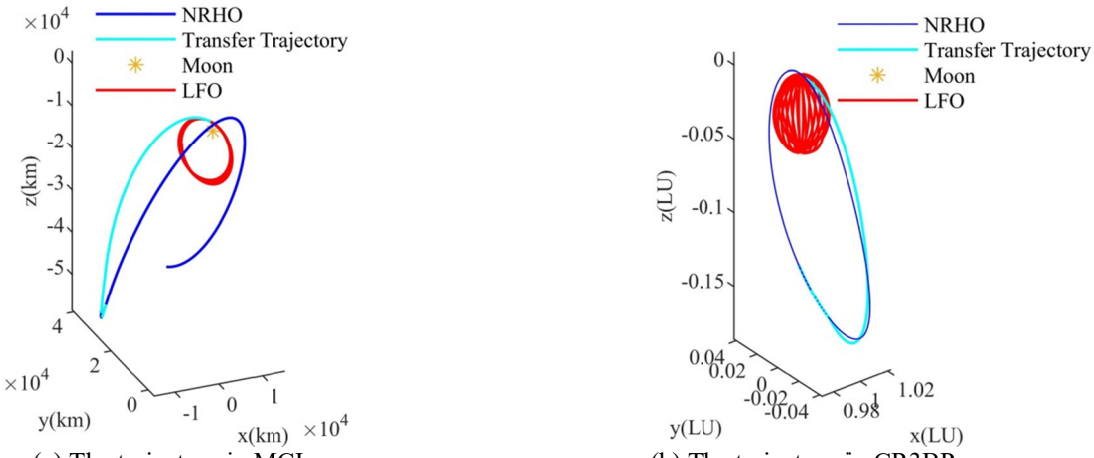

(a) The trajectory in MCI (b) The trajectory in CR3BP

Figure 4: The trajectories with the initial epoch of Jan 1 2026 (case 1)

DOI: 10.13009/EUCASS2025-235

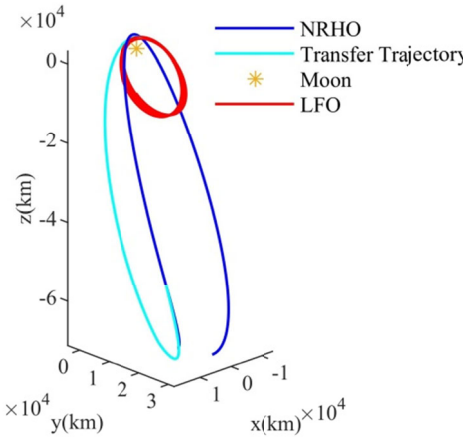

(a) The trajectory in MCI

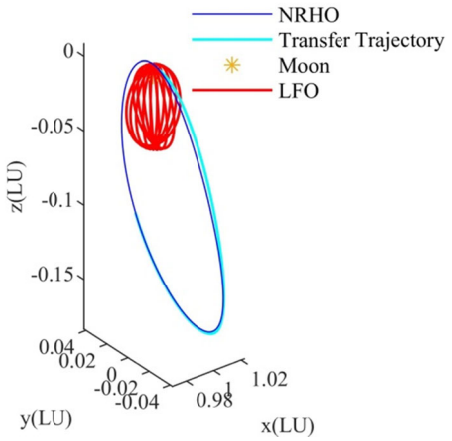

(b) The trajectory in CR3BP

Figure 5: The trajectories with the initial epoch of Jan 15 2026 (case 2)

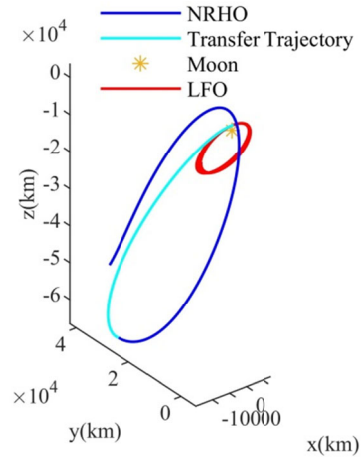

(a) The trajectory in MCI

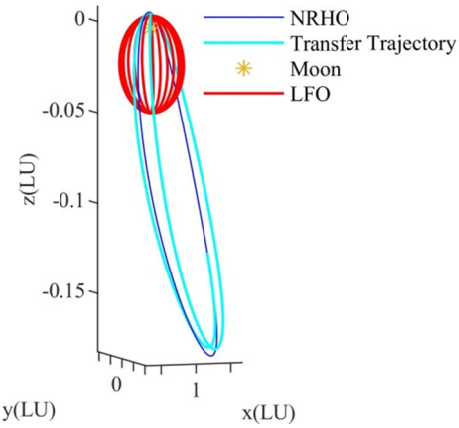

(b) The trajectory in CR3BP

Figure 6: The trajectories with the initial epoch of Feb 10 2026 (case 3)

The detailed optimization results are listed in Table 4.

Table 4: The optimization results of three cases

Case index	Total Δv, km/s	Transfer time, day	1st Δv, km/s	2nd Δv, km/s	3rd Δv, km/s
1	0.12399	4.7413	5.63403×10^{-5}	0.02021	0.10373
2	0.16667	5.3081	0.01442	0.02188	0.13036
3	0.12872	3.5338	3.61348×10^{-7}	0.02719	0.10153

Through optimization, three sets of transfer results are obtained near different initial epochs. The transfer times are all less than 10 days, which benefits from the stretching directions. The 1st Δv values are less than 20 m/s, which means that a small maneuver along the stretching direction is enough to drive the spacecraft away from the initial orbit rapidly. The largest portion of the Δv cost is used to insert into the LFO. This is due to the significant difference in orbital radius, which can also be seen from the trajectories. Overall, based on the transfer trajectory design method proposed in this paper, the Δv is used to overcome the energy difference between the two orbits, which means the method and results are reasonable. Therefore, the proposed method is proved to enable the acquisition of a rapid and efficient transfer trajectory from an NRHO to a LFO.

DOI: 10.13009/EUCASS2025-235

5. Conclusions

A novel design methodology of multi-impulse transfer trajectory from NRHOs to LFOs is proposed. The 9:2 NRHO and Sun-synchronized lunar frozen orbits are selected as the objects of the research. An optimization model for trajectory design is constructed, with transfer flight time, the orbital parameters of LFO, etc., as optimization variables. By optimally solving this constrained nonlinear optimization problem, the transfer trajectories under the CR3BP and high-fidelity models are obtained. In particular, applying the stretching direction strategy increases the efficiency of orbital transfer and can also reduce the number of design variables. Several trajectories are obtained by the proposed design method. Detailed results show that transfers between the two orbits can be accomplished rapidly (within several days) with a velocity increment of only 100–200 m/s. Trajectories designed under high-fidelity models have potential for engineering applications and can provide new mission orbits for future cislunar space missions.

Acknowledgments

This work was supported by the National Natural Science Foundation of China. (Nos. 12372046) and Natural science Foundation of Jiangsu Province (No. BK20220130).

References

[1] M. Smith, D. Craig, N. Herrmann, E. Mahoney, J. Krezel, N. Mclntyre. 2020. The artemis program: An overview of nasa's activities to return humans to the moon. In *2020 IEEE aerospace conference*. 1-10.
[2] L. Lu, H. Li, W. Zhou, J. Liu. 2021. Design and analysis of a direct transfer trajectory from a near rectilinear halo orbit to a low lunar orbit. *Advances in Space Research.* 67(3):1143-1154.
[3] H. Yang, J. Hu, X. Bai, S. Li. 2023. Review of trajectory design and optimization for Jovian system exploration. *Space: Science & Technology*. 3 0036.
[4] K. C. Howell, J. V. Breakwell. 1984. Almost rectilinear halo orbits. *Celestial mechanics*. 32:29-52.
[5] R. Whitley, R. Martinez. 2015. Options for staging orbits in cislunar space. In: *IEEE Aerospace Conference, Big Sky*. 1-9.
[6] V. Muralidharan, K. C. Howell. 2023. Stretching directions in cislunar space: Applications for departures and transfer design. *Astrodynamics*. 7(2):153-178
[7] S. Qin, Y. Huang, P. Li, Q. Shan, M. Fan, X. Hu, G. Wang. 2019. Orbit and tracking data evaluation of Chang'E-4 relay satellite. *Advances in Space Research*. 64(4):836-846.
[8] D. Guzzetti, E. M. Zimovan, K. C. Howell, D. C. Davis. 2017. Stationkeeping analysis for spacecraft in lunar near rectilinear halo orbits. In: *27th AAS/AIAA Space Flight Mechanics Meeting. American Astronautical Society*. 160:3199-3218.
[9] L. Liu, Y. Liu. 2025. A note on the computation of multi-revolution NRHO under the ephemeris model. *Advances in Space Research*. 75(3):2889-2907.
[10] S. Trofimov, M. Shirobokov, A. Tselousova, M. Ovchinnikov. 2020. Transfers from near-rectilinear halo orbits to low-perilune orbits and the Moon's surface. *Acta Astronautica*. 167: 260-271.
[11] L. Lu, H. Li. W. Zhou. J. Liu. 2021. Design and analysis of a direct transfer trajectory from a near rectilinear halo orbit to a low lunar orbit. *Advances in Space Research*. 67(3):1143-1154.
[12] K. Oshima. 2019. The use of vertical instability of L 1 and L 2 planar Lyapunov orbits for transfers from near rectilinear halo orbits to planar distant retrograde orbits in the Earth–Moon system. *Celestial Mechanics and Dynamical Astronomy*. 131(3):14.
[13] T. Nie, P. Gurfil. 2018. Lunar frozen orbits revisited. *Celestial Mechanics and Dynamical Astronomy*. 130(10):61.
[14] T. A. Ely. 2020. Stable constellations of frozen elliptical inclined lunar orbits. *Journal of Astronautical Sciences*. 53:301-316.
[15] G. Chen, S. Wu, J. You, Q., Zhang. 2024. Communication-navigation integrated satellite constellation for lunar exploration: Frozen-orbit based HyInc walker. *IEEE Journal on Selected Areas in Communications*. 42:1436-1452
[16] Z. Meng. 2024. Design of sun-synchronous and repeating tracking condition elliptical lunar frozen orbits. *Acta Aeronautica et Astronautica Sinica*. 45(18):229926(in Chinese).
[17] E. M. Zimovan-Spreen, K. C. Howell, C. C. Davis. 2020. Near rectilinear halo orbits and nearby higher-period dynamical structures: orbital stability and resonance properties. *Celestial Mechanics and Dynamical Astronomy*. 132(5): 28.